

## EVIDENCE OF EIT AND MORETON WAVES IN NUMERICAL SIMULATIONS

P. F. CHEN,<sup>1,2</sup> S. T. WU,<sup>3</sup> K. SHIBATA,<sup>2</sup> AND C. FANG<sup>1</sup>

Received 2002 February 1; accepted 2002 April 29; published 2002 May 14

### ABSTRACT

Solar coronal mass ejections (CMEs) are associated with many dynamical phenomena, among which EIT waves have always been a puzzle. In this Letter MHD processes of CME-induced wave phenomena are numerically simulated. It is shown that as the flux rope rises, a piston-driven shock is formed along the envelope of the expanding CME, which sweeps the solar surface as it propagates. We propose that the legs of the shock produce Moreton waves. Simultaneously, a slower moving wavelike structure, with an enhanced plasma region ahead, is discerned, which we propose corresponds to the observed EIT waves. The mechanism for EIT waves is therefore suggested, and their relation with Moreton waves and radio bursts is discussed.

*Subject headings:* Sun: activity — Sun: corona — Sun: magnetic fields — waves

### 1. INTRODUCTION

Solar coronal mass ejections (CMEs) are presently the largest known solar eruptive activity in spatial scale and also in energetics and geoeffectiveness. CMEs are associated with numerous dynamical phenomena with a wide range of spatial scales and observed at different wavelengths, e.g., emerging flux, filament eruptions, solar flares, type II radio bursts, Moreton waves, EIT dimming and waves, geomagnetic storms. Among them, the mechanism for EIT waves is still unclear.

EIT waves were discovered by the EUV Imaging Telescope (EIT) aboard the *Solar and Heliospheric Observatory (SOHO)* as transient wavelike structures with enhanced coronal emission that are followed by an expanding dimming region. They propagate nearly circularly from a flare site (Moses et al. 1997; Thompson et al. 1998) or inhomogeneously, avoiding strong magnetic features and neutral lines. Generally, they stop near coronal holes (Thompson et al. 1999). These authors suggested that the EIT waves are simply the coronal counterparts of chromospheric Moreton waves, although the velocities of the latter are generally 2–3 times larger (Smith & Harvey 1971; Klassen et al. 2000).

Following this line of thought, Wang (2000) found that the ray path of fast-mode waves matches the EIT bright fronts, including their slow expansion rate and their tendency to avoid active regions and coronal holes. Concerning the velocity discrepancy between Moreton and EIT waves, Wang (2000) proposed that the former are super-Alfvénic shocks, while the latter are just fast-mode waves. Recently, Wu et al. (2001) performed three-dimensional numerical simulations with a solar flare-induced pressure pulse, and they found that the fast wave fronts of the resulting perturbation reproduce many properties of the observed EIT waves. However, note that in both Wang (2000) and Wu et al. (2001) the magnetograms of the Wilcox Solar Observatory are used to extrapolate the coronal field, which results in coronal plasma  $\beta$ -values (ratio of gas to magnetic pressure) of higher than 1 in the quiet region where most EIT waves are observed. As Wu et al. (2001) pointed out, their consistency with the observations can be reached only if the coronal  $\beta$  is larger than 1. Such a large  $\beta$  is possible in the middle corona but unrealistic in the low corona (e.g., Gary 2001).

Furthermore, Delannée & Aulanier (1999) and Delannée (2000) pointed out that only three of 50 flares produced in the same active region were associated with EIT waves, indicating that flares are unlikely to be the primary cause of EIT waves. They proposed that the bright EIT front may be produced by the sudden expansion of a part of the magnetic field lines forming the separatrix when the flare occurs.

In this Letter MHD processes of CMEs are numerically simulated in order to reconcile all the discrepancies. In § 2 the numerical method is described. Results are shown in § 3. Discussion is presented in § 4, where the mechanism for EIT waves is proposed.

### 2. NUMERICAL METHOD

Two-dimensional, time-dependent, compressible resistive MHD equations in Cartesian coordinates are numerically solved by a multistep implicit scheme (Hu 1989) that was further developed by Chen, Fang, & Hu (2000). The equations can be found in Chen & Shibata (2000). Five independent dimensionless variables are density ( $\rho$ ), velocity ( $v_x, v_y$ ), magnetic flux function ( $\psi$ ), and temperature ( $T$ ); note that  $\mathbf{B} = \nabla \times \psi \hat{e}_z$ ,  $x$ -axis is horizontal, and  $y$ -axis is upward. The units of  $\rho$ ,  $T$ , and  $L$  are  $\rho_0 = 1.67 \times 10^{-12} \text{ kg m}^{-3}$ ,  $T_0 = 1.5 \times 10^6 \text{ K}$ , and  $L_0 = 10^5 \text{ km}$ , respectively.  $\beta_0$  is the plasma  $\beta$  at the reference point (3.5, 0).

The initial magnetic field consists of three components: a line current ( $\psi_l$ ), its image current ( $\psi_i$ ), and the background field ( $\psi_b$ ), where

$$\psi_i = \begin{cases} \frac{r^2}{2r_0}, & r \leq r_0, \\ \frac{r_0}{2} - r_0 \ln r_0 + r_0 \ln r, & r > r_0, \end{cases} \quad (1)$$

$$\psi_i = -\frac{r_0}{2} \ln [x^2 + (y + 2)^2], \quad (2)$$

$$\psi_b = 0.143$$

$$\times \ln \frac{[(x + 0.3)^2 + (y + 0.3)^2][(x - 0.3)^2 + (y + 0.3)^2]}{[(x + 15)^2 + (y + 0.3)^2][(x - 15)^2 + (y + 0.3)^2]}, \quad (3)$$

<sup>1</sup> Department of Astronomy, Nanjing University, 22 Hankou Lu, Nanjing, Jiangsu 210093, China; chenpf@kwasan.kyoto-u.ac.jp.

<sup>2</sup> Kwasan Observatory, Kyoto University, Yamashina, Kyoto 607-8471, Japan; shibata@kwasan.kyoto-u.ac.jp.

<sup>3</sup> Center for Space Plasma, Aeronomy, and Astrophysics, University of Alabama in Huntsville, Huntsville, AL 35899; wus@cspar.uah.edu.

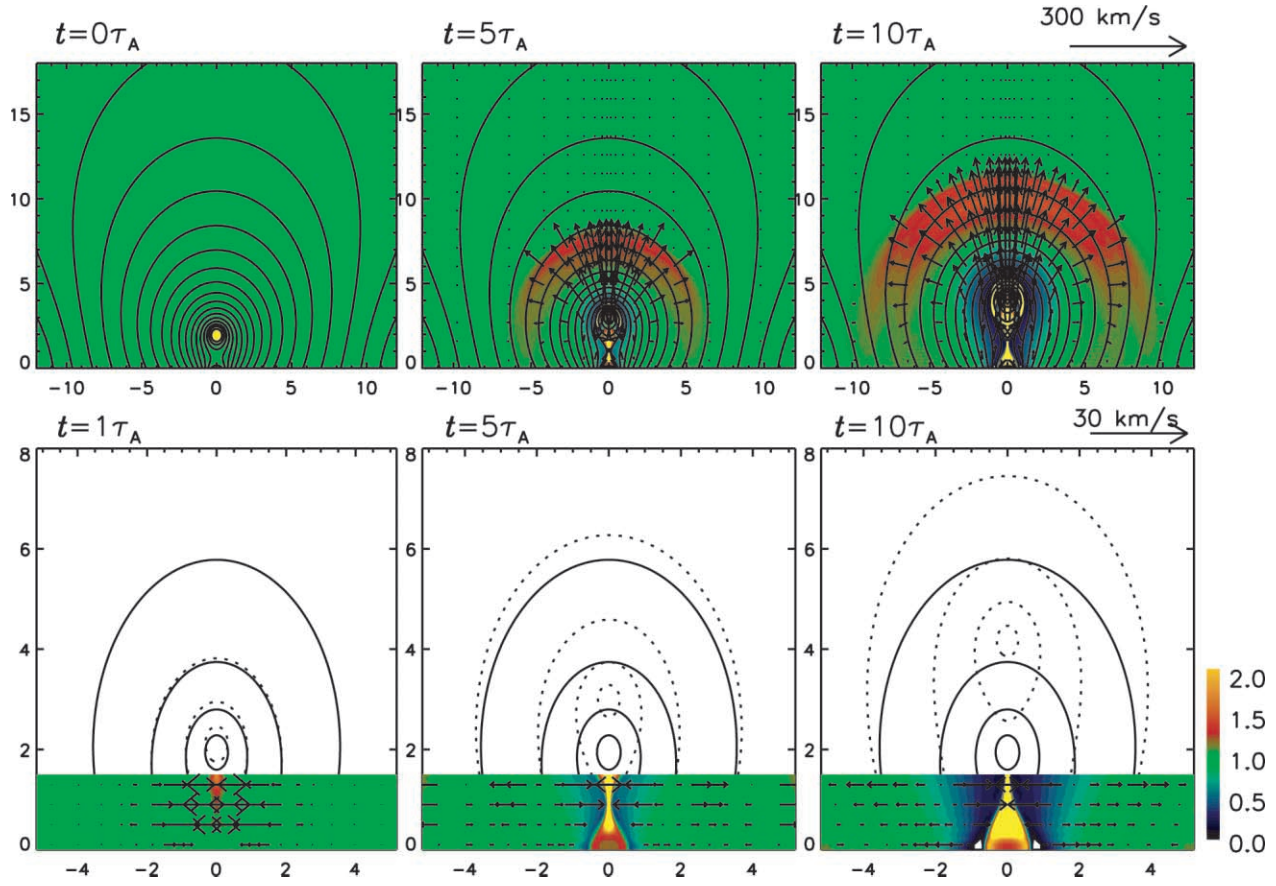


FIG. 1.—Case with  $\beta_0 = 0.25$  and  $v_{\text{rope}} = 100 \text{ km s}^{-1}$ . *Upper panels:* Global evolution of the density (color), magnetic field (solid lines), and velocity (arrows). *Lower panels:* Local evolution of the density (color), magnetic field (dotted lines), and horizontal velocity (arrows), where initial magnetic configuration is superposed as solid lines.

where  $r = [x^2 + (y - 2)^2]^{1/2}$  and  $r_0 = 0.5$ .

Initially, a uniform temperature  $T = 1$  is assumed. The density is distributed in order that the initial gas pressure can balance the magnetic force within the flux rope when the image current and the background field are absent (Chen & Shibata 2000).

To initiate CMEs, shearing motion, converging motion, or flux emergence is appropriate (see Chen & Shibata 2000). Here, similar to Magara et al. (2000), an upward external force  $\mathbf{F} = (1 - 0.967e^{-t})e^{\psi_c - \psi} \text{sgn}(v_{\text{rope}} - v_c)\hat{e}_y$  is exerted on the flux rope, i.e., the region with  $\psi \leq \psi_c + 1.768$ , where  $\psi_c$  is the value of  $\psi$  at the flux rope center,  $v_c$  is the velocity at the flux rope center, and  $v_{\text{rope}}$  is a parameter that controls the final velocity of the flux rope. The initial value  $\mathbf{F} = 0.033\hat{e}_y$  is chosen by trial and error to ensure the initial configuration remains stable for a long enough time. The resistivity  $\eta$  is locally distributed near the X-point below the flux rope as  $\eta = 0.05 \times \cos(1.5\pi x)\cos[\pi(y - y_n)]$  in the region  $|x| \leq 0.33$ ,  $|y - y_n| \leq 0.5$ , where  $y_n$  is the height of the reconnection X-point.

The dimensionless size of the simulation box is  $|x| \leq 12$  and  $0 \leq y \leq 18$ . Owing to symmetry, the simulations are made only in the right half region, which is discretized by  $82 \times 181$  grid points. The bottom of the simulation area is a line-tying boundary, where all quantities are fixed except for  $T$ , which is determined by equivalent extrapolation. The left boundary ( $x = 0$ ) is a symmetric one, while the other two are open ones.

### 3. NUMERICAL RESULTS

As the external force increases, the flux rope begins to rise. As indicated in Chen & Shibata (2000), the plasma below the

flux rope is evacuated, and the surrounding plasma with frozen-in field lines is driven inward to form a current sheet near the null point. Reconnection is then triggered. Below the reconnection X-point, cusp-shaped flare loops are formed as shown in Figure 1, which presents the evolution of density, magnetic field, and velocity for the case of  $\beta_0 = 0.25$  ( $\tau_A = 224 \text{ s}$ ) and  $v_{\text{rope}} = 100 \text{ km s}^{-1}$ . As the reconnection continues, the flare loop expands and its two footpoints separate, constituting the apparent motions of two-ribbon flares (see Chen et al. 1999). A piston-driven shock appears straddling over the flux rope, which moves upward at a speed of  $360 \text{ km s}^{-1}$  at  $t = 4\tau_A$ , larger than the local fast-mode wave velocity. Near the solar surface, the piston-driven shock may degenerate to a finite amplitude MHD fast wave (Wu et al. 2001).

Figure 2 depicts the evolution of the density distribution along the right half of the horizontal line  $y = 0.5$ . The density distribution at each time is stacked on the previous one with an increment of 0.018 every  $0.4\tau_A$ . In this figure, two wavelike structures are evident besides the motion of the flare loop footpoint. The first wave, which propagates very fast and lies at the outermost part of the perturbed region, corresponds to one leg of the piston-driven shock wave. It moves at  $\sim 400 \text{ km s}^{-1}$  near  $t = 4\tau_A$ . Between this wave and the flare loop footpoint is the second wave with a wide range of plasma enhancement, the left boundary of which becomes increasingly blurred. For the case in Figure 2, its propagation velocity is  $\sim 115 \text{ km s}^{-1}$  near  $t = 4\tau_A$ , and the maximum density enhancement is  $\sim 7\%$  at  $t = 17\tau_A$ .

Further simulations with the same  $\beta_0$  show that the  $\rho$  en-

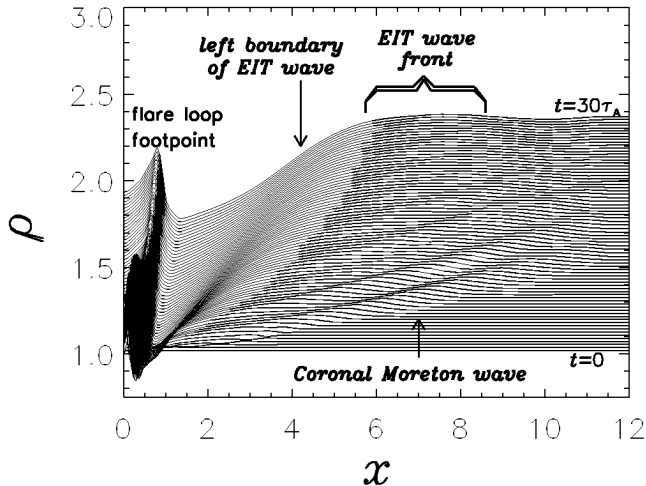


FIG. 2.—Evolution of the density ( $\rho$ ) distribution along the line  $y = 0.5$ . Note that the  $\rho$  distribution at each time is stacked on the previous one with an increment of 0.018 every  $0.4\tau_A$ .

hancement increases with increasing  $v_{\text{rope}}$ , but mostly it is smaller than 10%; the velocities of both the top and the extended legs of the piston-driven shock increase with increasing  $v_{\text{rope}}$ , while the velocity of the second wave hardly changes. Another case with  $\beta_0 = 0.05$  ( $v_A = 1000 \text{ km s}^{-1}$ ) and  $v_{\text{rope}} = 300 \text{ km s}^{-1}$  was simulated. In this case, near  $t = 4\tau_A$ , the piston-driven shock moves upward at  $885 \text{ km s}^{-1}$  (the local fast wave velocity is  $540 \text{ km s}^{-1}$ ). Its leg sweeps the horizontal line  $y = 0.5$  (i.e., the first wave) at a speed of  $773 \text{ km s}^{-1}$ , while the second wave propagates at  $250 \text{ km s}^{-1}$ .

To illustrate the physical meaning of the second wave, distributions of the running difference of the density ( $\Delta\rho$ ) and the  $x$ -component of velocity ( $v_x$ ) along the line  $y = 0.5$  are displayed in Figure 3. The running difference is derived from the distribution at each time by subtracting the previous one. In Figure 3 it can be seen again that the flare loop footpoint moves slowly rightward, and the leg of the piston-driven shock moves very fast. The left boundary of the second wave in Figure 2 corresponds in this figure to the interface between a dimming region and a  $\Delta\rho$  enhancement in the left panel and to the large positive  $v_x$ , i.e., strong expansion, in the right panel. Within the dimming region, the distribution of  $\Delta\rho$  is quite smooth while the  $\Delta\rho$  enhancement region is full of fast-moving waves. Note that these wave fronts, enlarged by the short time difference, may not be observed by *SOHO*/EIT.

#### 4. DISCUSSION

##### 4.1. Moreton Waves

Before the discovery of CMEs, it was found that  $\text{H}\alpha$  disturbances in some flare events propagate through the chromosphere over distances on the order of  $5 \times 10^5 \text{ km}$  with a velocity ranging from  $500$  to  $2000 \text{ km s}^{-1}$  (Moreton & Ramsey 1960). They could not be accounted for by any wave of chromospheric origin. Uchida (1968) proposed that the skirt of the wave front surface of the coronal fast-mode wave sweeps the chromosphere and produces the Moreton waves. This model can successfully explain the properties of Moreton waves. As further pointed out by Uchida (1974), a fast-mode coronal wave originating in an active region may sharpen into a super-Alfvénic fast-mode shock wave that emits type II radio bursts in the corona; therefore, Moreton waves and type II radio bursts

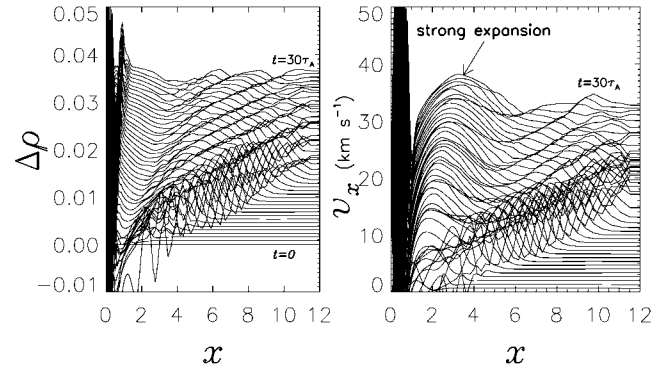


FIG. 3.—Evolutions of the running difference of density distribution ( $\Delta\rho$ ; left panel) and  $x$ -component velocity ( $v_x$ ; right panel) along the line  $y = 0.5$ . Note that the distribution at each time is stacked on the previous one with an increment of 0.00075 every  $0.6\tau_A$  for the left panel and with an increment of 0.66 every  $0.6\tau_A$  for the right panel.

should come from the same agent: the flare-produced coronal MHD fast-mode shock front. According to our results, the piston-driven shock, proposed as the type II radio burst source by Magara et al. (2000), appears to be straddling over the expanding CME and may sweep the chromosphere to produce the Moreton waves observed in  $\text{H}\alpha$ . However, note that the shock comes from the expanding CME, not from the flare itself, although the flare may accelerate the CME (Chen & Shibata 2000). We propose such a scenario: as the CME expands vertically and horizontally, a piston-driven shock is formed in front of it. As the eruption progresses, the legs of the fast-mode shock sweep the solar surface to form the Moreton waves.

##### 4.2. EIT Waves

Our numerical results show that a cusp-shaped flare is produced by the magnetic reconnection below the flux rope. The two footpoints of the flare loop separate with a velocity of tens of kilometers per second. This apparent motion is clearly seen in Figure 2 as a slowly moving structure. Between this structure and the coronal Moreton wave, another wavelike structure is identified as the left boundary of a propagating plasma enhancement. We propose that the propagating enhancement is the observed EIT wave front. According to the numerical results, the velocity of our EIT wave is about one-third of the corresponding coronal Moreton wave velocity. For example, in the case of  $\beta_0 = 0.05$  and  $v_{\text{rope}} = 300 \text{ km s}^{-1}$ , the EIT wave moves at  $250 \text{ km s}^{-1}$ , and the Moreton wave moves at  $773 \text{ km s}^{-1}$  near  $t = 4\tau_A$ . This is consistent with observations from statistical analysis (Smith & Harvey 1971; Klassen et al. 2000) and an individual event (e.g., Eto et al. 2002). Also, the inferred starting time of the EIT wave, extrapolated from the later evolution back to the flare site, would be earlier than the CME onset since its velocity is larger near the flare site than farther away, as shown in Figure 2. This is consistent with observations.

The mechanism of the EIT waves is revealed by Figure 3, where it is seen that the left boundary of the EIT wave fronts in Figure 2 always corresponds to the interface between a smooth dimming region on the left side and a fast-mode wave-propagating region on the right side in the left panel and to the strong expansion in the right panel. Therefore, each EIT wave front is just the source of a new perturbation that emits fast-mode waves. The underlying physical process is illustrated in Figure 4 (see also Fig. 1; lower panels): as the flux rope rises, the field line near point A is first deformed (i.e., opening

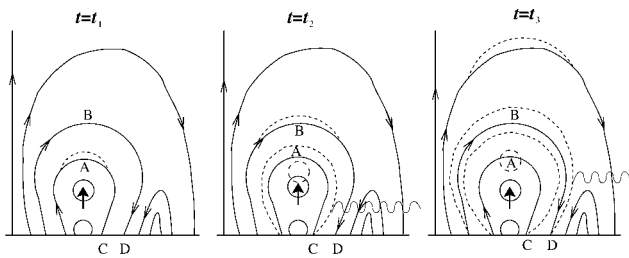


FIG. 4.—Propagation of EIT wave front from point C to point D, where the rising flux rope is the original source for the successive opening of all field lines. Solid lines represent the initial configuration; dashed lines correspond to the new configuration at each new time; wavy lines represent the fast-mode waves emitted from the EIT wave fronts. Moreton waves, much ahead of the EIT wave fronts, are not shown.

of the field line). The perturbation will propagate out with the phase velocity of fast-mode waves, or even shock waves, while the large-amplitude deformation itself will be transferred across the field lines up to point B and also along the field line down to point C by wave groups with their respective group velocities. Then, an EIT wave front appears at point C. Subsequently, the deformation at point B is transferred up and also down to point D with group velocities of waves. Thus, a new EIT wave front appears at point D, although the fast-mode waves emitted from point C have already passed point D traveling at the phase velocity. Therefore, successive opening of the field lines produces successive density enhancements on the outer side; i.e., successive EIT wave fronts are formed, and correspondingly, the plasma gets evacuated in the inner region, i.e., the dimming region. For simplicity we assume the field lines near the flare site are uniform concentric semicircles. Then, the time lag between the deformation near points D and C is  $\Delta t = AB/v_f + (BD - AC)/v_A$ , where  $v_f = (v_A^2 + c_s^2)^{1/2}$  and  $v_A$  are the group velocities across and along the field lines, respectively,  $v_A$  is the Alfvén speed, and  $c_s$  is the sound speed (Priest 1982, p. 169). We deduce that the apparent velocity of the EIT waves is  $v_{\text{EIT}} = CD/\Delta t = 1/(1/v_f + \pi/2v_A) \sim 0.34v_f$  (where  $v_A = 0.8v_f$  is assumed). Since the coronal Moreton waves (weak MHD shock waves) propagate with a velocity of  $\sim v_f$ , this analytic result implies that EIT waves move at a velocity of about 0.34 times their corresponding Moreton waves, which is roughly consistent with observations and our simulations. Outside the active region,  $v_f$  gets smaller and the coronal field lines are prolate or partially open rather than semicircles. Therefore,  $\Delta t$  is larger—it even gets infinite toward the fully open field lines—and the EIT waves move slower in quiet regions than near the flare site and even stop at the boundaries of coronal holes (with open field lines) as indicated by Thompson et al. (1999).

As seen in the above analysis, the velocity of EIT waves is about 0.34 times the fast-mode wave velocity, which is not related to the rising velocity of the flux rope, as also indicated in § 3. On the contrary, the motion of the piston-driven shock above the flux rope, which emits type II radio bursts, is strongly related to the rising velocity of the flux rope. That is, the faster the rope moves, the larger Mach number the shock has and the faster the shock wave moves. This characteristic could well explain the lack of correlation between the velocities of type II radio bursts and EIT waves discovered by Klassen et al. (2000). Similar to Wu et al. (2001), when encountering another strong active region disconnected by a separatrix, EIT waves will stop since the opening of field lines is terminated.

In summary, our results indicate that a piston-driven shock, induced by the rising flux rope, straddles over the expanding CME, and its legs sweep the chromosphere to produce Moreton waves. Moreover, a new interpretation of EIT waves is presented: they are formed by successive opening of the field lines covering the flux rope. The successive opening is transferred by wave groups. More precisely, EIT waves are not real waves but the propagation of perturbation sources. In this sense, our theory is different from that of Wang (2000) and Wu et al. (2001), who treat EIT waves as fast-mode waves, and is similar to that of Delannée & Aulanier (1999), who attribute EIT waves to the evolution of magnetic field lines associated with separatrices. Our theory implies that all the field lines covering the flux rope are opened successively to form the apparent propagation of EIT wave fronts. Contrary to the model of Wang (2000) and Wu et al. (2001), which requires high-plasma  $\beta$  in the corona, only a small value of  $\beta$  in our model can reproduce the observed velocities of EIT waves.

Note that the downward extension of the piston-driven shock would sweep the lower corona before sweeping the chromosphere. Therefore, it is possible to observe a true EIT wave that is the real coronal counterpart of the Moreton wave. This may have been observed by Warmuth et al. (2001), although the temporal resolution of *SOHO*/EIT ( $\sim 15$  minutes) is not sufficiently high. However, it is expected that the real EIT wave should have a much sharper wave front than the general blurry “EIT wave.”

The authors thank T. Holzer, J. Wang, S. Wang, and D. Brooks for discussions and an anonymous referee for constructive comments. The visit of P. F. C. to Kyoto University is supported by the Japan Society for the Promotion of Science. This research is also supported by NSFC (49990451 and 19973009) and NKBRFS (G20000784). S. T. W. is supported by NSF (ATM 00-70385) and AFOSR (F49620-00-0-0204).

#### REFERENCES

- Chen, P. F., Fang, C., Ding, M. D., & Tang, Y. H. 1999, *ApJ*, 520, 853  
 Chen, P. F., Fang, C., & Hu, Y. Q. 2000, *Chinese Sci. Bull.*, 45, 798  
 Chen, P. F., & Shibata, K. 2000, *ApJ*, 545, 524  
 Delannée, C. 2000, *ApJ*, 545, 512  
 Delannée, C., & Aulanier, G. 1999, *Sol. Phys.*, 190, 107  
 Eto, S., et al. 2002, *PASJ*, in press  
 Gary, G. A. 2001, *Sol. Phys.*, 203, 71  
 Hu, Y. Q. 1989, *J. Comput. Phys.*, 84, 441  
 Klassen, A., Aurass, H., Mann, G., & Thompson, B. J. 2000, *A&AS*, 141, 357  
 Magara, T., Chen, P. F., Shibata, K., & Yokoyama, T. 2000, *ApJ*, 538, L175  
 Moreton, G. E., & Ramsey, H. E. 1960, *PASP*, 72, 357  
 Moses, D., et al. 1997, *Sol. Phys.*, 175, 571  
 Priest, E. R. 1982, in *Solar Magnetohydrodynamics* (Dordrecht: Riedel)  
 Smith, S. F., & Harvey, K. L. 1971, in *Physics of the Solar Corona*, ed. C. J. Macris (Dordrecht: Reidel), 156  
 Thompson, B. J., et al. 1998, *Geophys. Res. Lett.*, 25, 2465  
 ———. 1999, *ApJ*, 517, L151  
 Uchida, Y. 1968, *Sol. Phys.*, 4, 30  
 ———. 1974, *Sol. Phys.*, 39, 431  
 Wang, Y.-M. 2000, *ApJ*, 543, L89  
 Warmuth, A., Vrsnak, B., Aurass, H., & Hanslmeier, A. 2001, *ApJ*, 560, L105  
 Wu, S. T., et al. 2001, *J. Geophys. Res.*, 106, 25,089